Aging effects on thermal conductivity of glass-forming liquids

Pranab Jyoti Bhuyan,[1,*] Rituparno Mandal,[1,†] Pinaki Chaudhuri,[2,‡] Abhishek Dhar,[3,§] and Chandan Dasgupta[1,3,‖]
[1]*Department of Physics, Indian Institute of Science, Bangalore 560012, India*
[2]*The Institute of Mathematical Sciences, Chennai 600113, India*
[3]*International Centre for Theoretical Sciences, TIFR, Bangalore 560089, India*

(Received 4 April 2017; revised manuscript received 30 January 2018; accepted 23 January 2020; published 21 February 2020)

Thermal conductivity of a model glass-forming system in the liquid and glass states is studied using extensive numerical simulations. We show that near the glass transition temperature, where the structural relaxation time becomes very long, the measured thermal conductivity decreases with increasing age. Second, the thermal conductivity of the disordered solid obtained at low temperatures is found to depend on the cooling rate with which it was prepared. For the cooling rates accessible in simulations, lower cooling rates lead to lower thermal conductivity. Our analysis links this decrease of the thermal conductivity with increased exploration of lower-energy inherent structures of the underlying potential energy landscape. Further, we show that the lowering of conductivity for lower-energy inherent structures is related to the high-frequency harmonic modes associated with the inherent structure being less extended. Possible effects of considering relatively small systems and fast cooling rates in the simulations are discussed.

DOI: 10.1103/PhysRevE.101.022125

I. INTRODUCTION

Thermal conductivity is an important material property, with wide-ranging applications, and understanding the mechanism of heat transport in different materials is crucial from both theoretical and applied perspectives. It is well known that crystalline materials transport heat more efficiently than glassy and disordered materials, for which the thermal conductivity (κ) can be orders of magnitude smaller [1,2].

A well-studied feature of glassy systems is the temperature (T)-dependence of their thermal conductivity, which is very distinct from that of crystals. One typically finds $\kappa \sim T^2$ at very low temperatures, followed by a pronounced plateau and then an eventual gradual increase with temperature. The low temperature features are expected to be of quantum-mechanical origin, and a range of mechanisms have been proposed to explain them [3–5]. One scenario relates the plateau to the presence of excess modes, the so-called *boson peak*, in the low-frequency regime of the vibrational spectrum of glasses [6–8], which has thereafter been connected with the presence of elastic heterogeneities in such materials [9,10].

More recently, a number of studies have looked at higher temperatures where classical physics dominates. This includes regimes much below the glass transition temperature where the system gets stuck in the basin of a low-energy *inherent structure* (IS) (local minimum of the potential energy), as well as intermediate temperatures where the system evolves slowly while undergoing transitions between different basins. In the former case, the system can be effectively described by a disordered harmonic model obtained by expanding the many-body potential about the minimum. Heat transport is then related to the diffusivity associated with the normal modes of the harmonic solid [11,12]. In the context of the jamming transition, the change in the form of the diffusivity in a soft-sphere packing was studied in [8,13,14], and a crossover was observed near the boson-peak frequency as the transition was approached. In Ref. [15], it was shown that the introduction of polydispersity leads to an amorphization transition, whereby the thermal conductivity of the system decreases considerably.

It is well-known that the material properties of glasses depend on their age and history of preparation, e.g., the cooling rate by which they were quenched from a fluid phase [16–18]. This dependence on the history can be seen, for example, in the transient response of glasses to applied shear [19–21]. Surprisingly, the question as to whether thermal transport in glasses depends upon the age of the material, or on the cooling rate used in its preparation, has not been explored. There is no systematic study for this question and this is one of the main issues that is addressed in the present work. Using extensive equilibrium and nonequilibrium simulations of a model structural glass former, we show that the thermal conductivity does depend on the age of the glass, and on the rate of cooling during preparation. Furthermore, we provide evidence that the decrease of thermal conductivity in glasses with growing age or slower cooling rate is linked to the exploration of ISs with lower energy. Apart from direct numerical simulations to monitor the thermal conductivity, we also investigate the glassy system in the harmonic approximation where we study the properties of the Hessian matrix related to small oscillations around a local minimum (IS).

*pranab@iisc.ac.in
†rituparno@iisc.ac.in
‡pinakic@imsc.res.in
§abhishek.dhar@icts.res.in
‖cdgupta@iisc.ac.in

By calculating the participation ratio and diffusivity of the normal modes associated with different ISs, we ask whether the decrease in κ can be related to an increase in the degree of localization of the vibrational modes. While some correlation is found, our results on this are not conclusive.

The paper is organized as follows. In Sec. II we describe the model system used in our simulation, and the nonequilibrium and equilibrium simulation schemes. In Sec. III we present the results of the simulations. We present the discussion of the harmonic approximation in Sec. IV. A concluding discussion is provided in Sec. V where we summarize the main results and discuss possible artifacts arising from the use of small systems and fast cooling rates in the simulations. Results of a harmonic calculation of the frequency and lifetime of phonon modes in our finite-size samples are presented in the Appendices.

II. MODEL AND METHODS

We consider the well-known model glass former—the Kob-Andersen binary Lennard-Jones mixture [22]. This model glass former consists of 80:20 proportion of A-type and B-type particles, all having unit mass, and interacting via the pair potential of the form

$$V_{ij}(r) = 4\epsilon_{ij}\left[\left(\frac{\sigma_{ij}}{r}\right)^{12} - \left(\frac{\sigma_{ij}}{r}\right)^{6}\right], \tag{1}$$

where $r = r_{ij}$ is the distance between the ith and the jth particle and the indices i, j can be A or B. The values of σ_{ij} and ϵ_{ij} are chosen to be: $\sigma_{AB} = 0.8\sigma_{AA}$, $\sigma_{BB} = 0.88\sigma_{AA}$, $\epsilon_{AB} = 1.5\epsilon_{AA}$, $\epsilon_{BB} = 0.5\epsilon_{AA}$. The potential is cut off at $r_{ij}^c = 2.5\sigma_{ij}$ and shifted accordingly using a smoothing function. The units of length and energy are set by $\sigma_{AA} = 1$ and $\epsilon_{AA} = 1$. Our study is done at a number density ($\rho = N/(L_xL_yL_z)$) of 1.2, where N is the number of particles within the simulation box of dimensions $L_x \times L_y \times L_z$. At this density, the Vogel-Fulcher-Tamman (VFT) transition temperature is $T_0 \approx 0.3$ in reduced Lennard-Jones units. We compute the thermal conductivity at different temperatures above and below this glass transition temperature. The supercooled liquid and glassy states we have studied were obtained via a well-defined cooling protocol [23]. The system is well-equilibrated at a high temperature ($T = 2.50$) in its liquid state and then cooled to a low temperature through a number of intermediate temperature steps. The number of intermediate steps and the amount of time spent in each step determine the cooling rate [23] of preparation. The numerical integration of the equations of motion are done using the velocity-Verlet algorithm.

A. Measuring thermal conductivity

Denoting the position and the velocity of the lth particle by $\vec{r}_l = \{r_l^\alpha\}$ and $\vec{v}_l = \{v_l^\alpha\}$ respectively (where $\alpha = x, y, z$), the energy current density at point $\vec{r}$ is given by [24]

$$\mathcal{J}^\alpha(\vec{r}, t) = \sum_l \delta(\vec{r} - \vec{r}_l)\left[\epsilon_l v_l^\alpha + \frac{1}{2}\sum_{n\neq l}\left(r_l^\alpha - r_n^\alpha\right) j_{l,n}\right], \tag{2}$$

where $\epsilon_l = \mathbf{v}_l^2/2 + (1/2)\sum_{n\neq l} V(r_{ln})$ is the energy of the lth particle, and $j_{l,n} = \frac{1}{2}\sum_v (v_l^v + v_n^v) f_{ln}^v$, with $f_{ln}^\alpha = -\partial V(r_{ln})/\partial r_l^\alpha$. We evaluated the thermal conductivity by several methods, which we now describe.

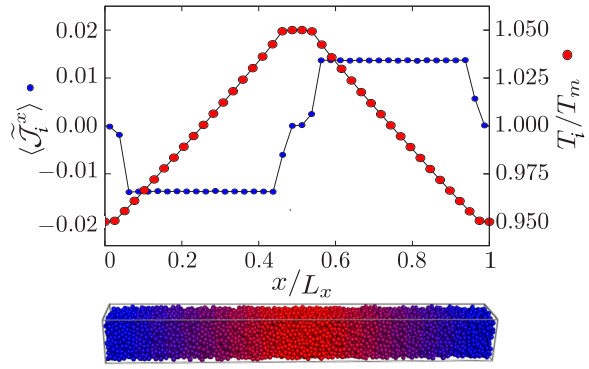

FIG. 1. (Top) Representative plot of local heat current density ($\langle\widetilde{\mathcal{J}}_i^x\rangle$) and reduced temperature (T_i/T_m) profile along the system, where T_m is the mean temperature of the sample in NEMD simulation; data is shown for a system of $N = 10\,000$ particles in a box with $L_y = L_z = 9.41$ and $L_x = 10 \times L_z$ at $T_m = 0.5$. (Bottom) Schematic diagram of the NEMD setup; the color red represents the hotter regions and blue represents the colder regions.

B. Nonequilibrium method (NEMD)

We consider a rectangular geometry, having the longer length L_x and cross-sectional lengths $L_y = L_z$, with periodic boundary conditions maintained in all directions as shown in Fig. 1. We consider a system with mean temperature T_m, impose a small temperature difference ΔT in the x direction across length $L_x' < L_x$, and measure the average steady-state heat current density $\langle\mathcal{J}^x\rangle = \frac{1}{V}\int_V d\vec{r}\langle\mathcal{J}^x(\vec{r}, t)\rangle$ where V is the volume of the region in the sample where the measurement is made. The thermal conductivity is then given by

$$\kappa = \frac{\langle\mathcal{J}^x\rangle \times L_x'}{\Delta T}. \tag{3}$$

We first prepare the initial equilibrium states (at mean temperatures T_m) via the cooling protocol discussed above. A temperature gradient was then applied by keeping a heat source at temperature $1.05T_m$ in a region of width $L_x/10$ in the middle of the system, and two heat sinks each of width $L_x/20$ at the two ends at $0.95T_m$. The thermostating of the hot and cold reservoirs was done by drawing the velocities of the particles in each reservoir from a Maxwell-Boltzmann distribution at the appropriate temperatures, at intervals of time 0.1. After an initial transient period following the imposition of the thermal gradient, the system reaches a nonequilibrium steady state. Typically, these timescales are relatively fast. Nevertheless, to definitely ensure steady-state sampling, we wait $\delta t \sim 10^4$ whereafter the typical spatial profiles of local temperature and heat current density are obtained. The spatial variation of the local temperature T_i and the local heat current density $\langle\widetilde{\mathcal{J}}_i^x\rangle$ was obtained by binning L_x into 40 segments, labeled $i = 1, \ldots 40$, and doing the averages separately for each segment over $\delta t \sim 5 \times 10^4$, after the transient time.

The bulk thermal conductivity (κ) of the system, at temperature T_m, is calculated from Eq. (3), using the average heat

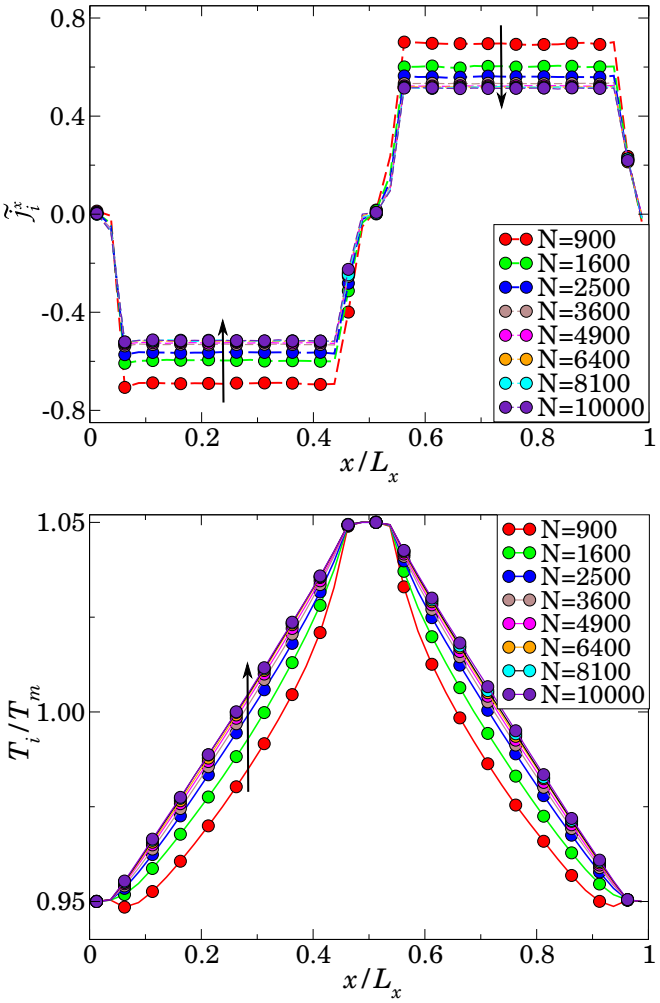

FIG. 2. (Top) $\tilde{j}_i^x$ and (bottom) reduced temperature (T_i/T_m) profile in the x direction for different system sizes (increasing size indicated by arrows) at $T_m = 0.5$. (Here, T_m is the mean temperature of the sample in nonequilibrium simulation). The different systems have an equal length ($L_x = 100a = 94.1$) along the direction of temperature gradient, and varying cross-sectional lengths $L_y(= L_z) =: 3a(N = 900), 4a(N = 1\,600), 5a(N = 2\,500), 6a(N = 3\,600), 7a(N = 4\,900), 8a(N = 6\,400), 9a(N = 8\,100)$, and $10a$ $(N = 10\,000)$.

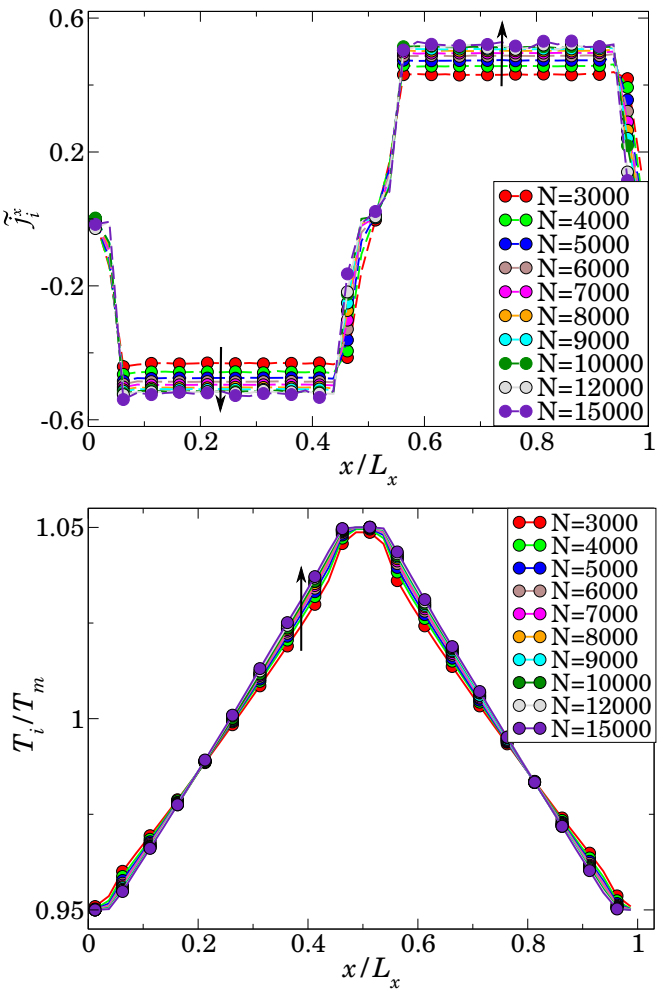

FIG. 3. (Top) $\tilde{j}_i^x$ and (bottom) reduced temperature (T_i/T_m) profile in the x direction for different system sizes (increasing size indicated by arrows) at $T_m = 0.5$. (Here, T_m is the mean temperature of the sample in nonequilibrium simulation). The different systems have equal cross-sectional lengths ($L_y = L_z = 10a = 9.41$), and varying lengths (L_x) along the direction of temperature gradient. $L_x =: 30a(N = 3\,000), 40a(N = 4\,000), 50a(N = 5\,000), 60a$ $(N = 6\,000), 70a(N = 7\,000), 80a(N = 8\,000), 90a(N = 9\,000)$, $100a(N = 10\,000), 120a(N = 12\,000)$, and $150a(N = 15\,000)$.

current density $\langle \mathcal{J}_x \rangle$ measured over the volume ($v' = L_x' L_y L_z$) of the region of the sample across which the temperature gradient is imposed. We define the local quantity $\tilde{j}_i^x$ in terms of the local heat current density $\langle \tilde{\mathcal{J}}_i^x \rangle$ as

$$\tilde{j}_i^x = \langle \tilde{\mathcal{J}}_i^x \rangle \times L_x'. \tag{4}$$

We have done averages over 32–160 independent MD trajectories for each state point, depending on temperature. While calculating the local quantities for a given segment we consider only the particles which are inside it, but the interaction of them with all other particles are taken into account.

We have investigated the effects of finite size of the system on κ in nonequilibrium simulations. In the following, we use $a = 0.941 \times \sigma_{AA} = 0.941$ and express the size of the simulation boxes in units of a.

1. Varying cross sections

We use simulation boxes with a fixed length ($L_x = 100a$) along the direction of temperature gradient and different cross sections with $L_y = L_z$. The top panel of Fig. 2 shows $\tilde{j}_i^x$ and in the bottom panel the temperature profile (T_i/T_m) along L_x is shown. We see that, for systems with $L_y(= L_z) \sim 6a\,(N = 3\,600)$, finite-size effects become negligible.

2. Varying lengths

We fix the cross-sectional lengths of the simulation box at $L_y = L_z = 10a$ and use systems of different length L_x along the directions of temperature gradient. The top panel of Fig. 3 shows $\tilde{j}_i^x$ and the bottom panel shows the temperature profile in the system. For systems with $L_x \sim 80a\,(N = 8\,000)$, the system-size effects become negligible.

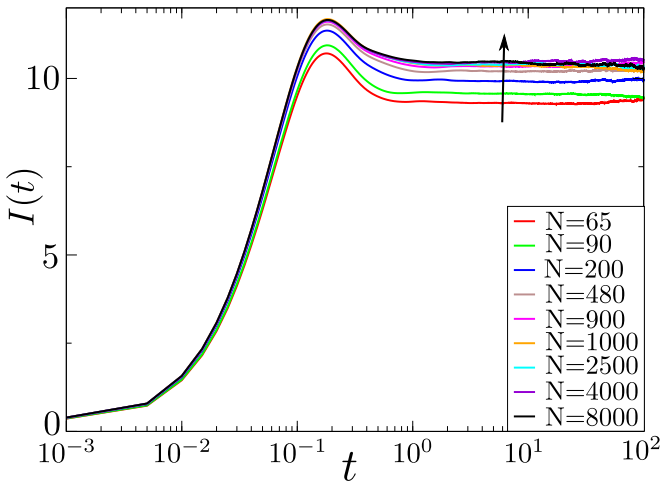

FIG. 4. $I(t)$ for different system sizes (increasing size indicated by arrow) at $T = 0.5$. The long time limit of $I(t)$ becomes independent of system sizes for $N \geqslant 900$.

For all further analysis using this nonequilibrium method, we choose the system specification of $L_y = L_z = 9.41$ and $L_x = 10 \times L_z$, which, thus, avoids any finite-size-related issues.

C. Green-Kubo method (EMD)

Alternatively, κ can be calculated using the Green-Kubo relation [24]:

$$\kappa = \frac{1}{3k_B T^2} \lim_{\tau\to\infty} \lim_{V\to\infty} \frac{\rho}{N} \int_0^\tau dt \langle \vec{\mathcal{J}}_{\rm tot}(0) \cdot \vec{\mathcal{J}}_{\rm tot}(t) \rangle, \quad (5)$$

where $\vec{\mathcal{J}}_{\rm tot}(t)$ is the integral of the heat current density $\vec{\mathcal{J}}(\vec{r}, t)$ over the whole system and the time correlation function is evaluated at equilibrium.

For the Green-Kubo calculation, we considered a cubic simulation box. An initial equilibrium state is prepared following the cooling protocol described earlier, and subsequently the NVE dynamics is switched on. The fluctuations of the heat current are then measured over a time-window of $\delta t \sim 10^4$ as the system evolves. The estimates of κ were obtained via averages over 96–384 independent trajectories.

Based on the conductivity formula for κ in Eq. (5), let us define the following quantity:

$$I(t) = \frac{1}{3k_B T^2} \frac{\rho}{N} \int_0^t dt' \langle \vec{\mathcal{J}}_{\rm tot}(0) \cdot \vec{\mathcal{J}}_{\rm tot}(t') \rangle. \quad (6)$$

In Fig. 4, we show the plots of $I(t)$ for different system sizes. The values of conductivity κ are calculated by appropriate averaging in the long time limit of $I(t)$. For a simulation box with $N \geqslant 900$, finite-size effects are found to be negligible. For most part of our analysis, we thus choose a system size of $N = 1\,000$.

III. SIMULATION RESULTS AND COMPARISON OF DIFFERENT METHODS

In Fig. 5(a), we compare the values of κ measured via the two schemes outlined above, for a given cooling rate. As expected for a disordered system, the magnitude of the thermal conductivity continuously decreases over the entire temperature range, before nearly saturating at very low temperatures. We observe very good agreement between the two different measurements of κ (using NEMD and EMD) over a very broad range of temperatures. Surprisingly, this is true even in the glassy regime, where the two methods provide the same result for states which have the same preparation history, i.e., produced via the same cooling rate. In the rest of the work we have used these two methods independently, in accordance with the question to be addressed. By performing simulations at various system sizes (keeping ρ constant), we have verified that the results for κ become essentially independent of system size for $N \sim 10^3$ (EMD) and $N \sim 10^4$ (NEMD). In the inset of Fig. 5(a) we show the system-size dependence of κ.

A. Effect of cooling rate

It is known that the cooling rate influences the glassy state obtained at low temperatures [18]. For example, the

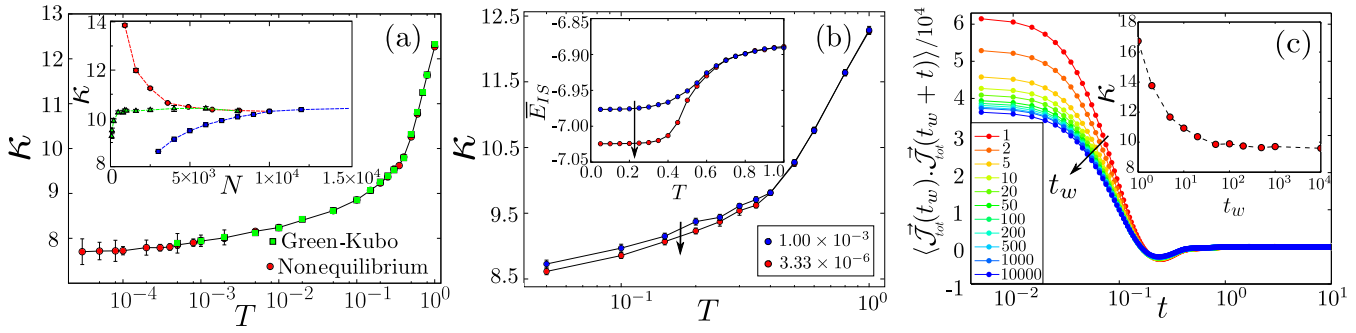

FIG. 5. (a) Comparison of thermal conductivity (κ) values obtained from NEMD simulation and EMD Green-Kubo calculation across a wide temperature range, using samples prepared with a cooling rate of 3.3×10^{-6}. (Inset) N dependence of κ: NEMD with varying L_x (blue, lower plot), varying $L_y (= L_z)$ (red, upper plot), and EMD with varying $L_x (= L_y = L_z)$ (green, middle plot). (For NEMD $T \equiv T_m$). (b) Variation of κ with temperature $T (\equiv T_m)$, from NEMD, using samples prepared via two different cooling rates as marked (arrow points to decreasing cooling rate). (Inset) Mean energy of ISs ($\overline{E}_{\rm IS}$) sampled at T for these cooling rates. Data is for $N = 10\,000$ with $L_y = L_z = 9.41$ and $L_x = 10 \times L_z$. (c) Heat current time auto-correlation function $\langle \vec{\mathcal{J}}_{\rm tot}(t_w) \cdot \vec{\mathcal{J}}_{\rm tot}(t_w + t) \rangle$ with changing age, t_w, using $N = 1\,000$ and $L_x = L_y = L_z = 9.41$, quenched from $T = 2.50$ to $T = 0.30$. (Inset) Variation of κ with t_w.

mean energy of the underlying ISs, $\overline{E}_{\rm IS}$, corresponding to any temperature, depends on the choice of the cooling rate [23], with slower cooling leading to exploration of lower energy ISs. Using data from our simulations, this is illustrated in the inset of Fig. 5(b), where we see that below a certain temperature, the variation of $\overline{E}_{\rm IS}$ with T branches out for two contrasting cooling rates. In the same spirit, we check how κ (from nonequilibrium measurements) varies with temperatures along the same two cooling branches. This is shown in Fig. 5(b), and we observe that the slower cooling corresponds to lower values of κ. However, compared to the data shown for $\overline{E}_{\rm IS}$ where the branching occurs at around $T = 0.55$, in the case of κ, the branching occurs at around $T = 0.40$ [see Fig. 5(b)], typically where the dynamics is known to fall out of equilibrium [18].

B. Effect of aging

The dependence of thermal conductivity on the history of preparation of the glassy state, as demonstrated above, implies that κ would also vary with the age of the glass when the system evolves after a thermal quench from high temperature to low temperatures. To investigate this, we quench the system from $T = 2.50$ to $T = 0.30$ (which is close to the VFT transition temperature) and let the system evolve in a constant temperature environment for a time t_w. Once the system has reached the age t_w, the NVE dynamics is switched on. Under such conditions, we measure the total heat current and calculate the corresponding autocorrelation function $\langle \vec{\mathcal{J}}_{\rm tot}(t_w) \cdot \vec{\mathcal{J}}_{\rm tot}(t_w + t)\rangle$. In Fig. 5(c), we show the current auto-correlation function for increasing age t_w. Note that the correlators relax quickly in time, even though the structural relaxations are extremely slow at this temperature [25]. The variation of conductivity κ with changing age t_w, calculated from these correlation functions using the Green-Kubo formula, is shown in the inset of Fig. 5(c): with increasing age, the thermal conductivity decreases. Now, it is known that, with increasing age, glassy systems visit deeper minima in the potential energy landscape [26]. It is also well-known [27] that low-temperature physical properties of glass-forming liquids and glasses are closely related to those of the ISs visited by the system during its time evolution. Therefore, the observed dependence of κ on t_w and our earlier observation regarding the dependence of κ on cooling rates are expected to be related to changes in the properties of the ISs visited by the system as the aging time and the cooling rate are changed.

C. Dependence on $E_{\rm IS}$

We now explore this possible link between properties of ISs and the values of κ. We consider a number of ISs with mean energy $\overline{E}_{\rm IS}$ and standard deviation $\sim 10^{-5}$ and prepare low temperature ($T = 0.002$) initial states for $N = 8\,000$ consistent with small harmonic fluctuations around the potential minimum. Using these states, MD simulations within the NVE ensemble are carried out. For the states that remain confined to the basin of the initial IS during the course of the simulation, the thermal conductivity is calculated using the Green-Kubo method. In Fig. 6, we show the dependence of κ on the energy of the IS; we find tha κ increases linearly

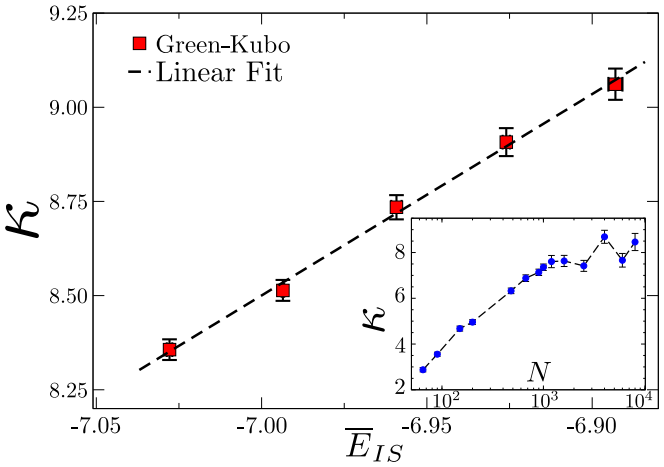

FIG. 6. Conductivity (κ) as a function of mean IS energy ($\overline{E}_{\rm IS}$) from low temperature Green-Kubo simulation starting with IS configurations, for $N = 8\,000$. The dashed line is a linear fit to the simulation data. (Inset) Dependence of κ on system size, from the Green-Kubo calculations.

with $\overline{E}_{\rm IS}$. In the inset of Fig. 6, we show the dependence of κ on the system size N. For large N, the values of κ exhibit large fluctuations about a value that does not show a strong dependence on N. We do not have a clear explanation of this behavior. It is possible that these fluctuations reflect the contribution of new phonon modes that appear as the system size is increased. As shown in Ref. [28], long-wavelength phonon modes appear as distinct spikes in the vibrational density of states. The appearance of a new spike as the system size is increased may cause a sharp change in the thermal conductivity. Also, our error bars involve several sources, such as sample-to-sample fluctuations and the inaccuracies in evaluation of the Green-Kubo integral, and it is possible that we have somewhat under-estimated the actual errors. In particular, the numerical difficulty in equilibrating large systems at low temperatures prevents us from obtaining good statistical sampling of inherent structures with low energy, which makes it difficult to obtain a reliable estimate of error bars from sample-to-sample fluctuations. However the trend we observe for the dependence of κ on the IS energy is quite robust. This result thus relates the observed decrease of the thermal conductivity with slower cooling, or with increasing age of the system after the thermal quench, to the exploration of ISs with lower energy.

IV. THE HARMONIC APPROXIMATION

A. Properties of harmonic excitations

At very low temperatures, the system mostly remains close to an IS of its potential energy landscape and one can approximate its potential energy to that of a harmonic solid. It is of interest to relate the thermal conductivity to the properties of the harmonic excitations, especially the effect of Anderson localization [29–31]. An expansion of the potential energy to quadratic order in the displacements from the IS gives the Hessian matrix which completely describes the properties of the harmonic solid. We ask how the properties of the

eigenvalues and eigenfunctions of the Hessian matrix affect thermal transport and the relation between κ and $\overline{E}_{\rm IS}$.

Following the formulation in Ref. [12], the thermal conductivity κ (from the Green-Kubo formula) for a harmonic system at temperature T can be expressed in terms of the *heat diffusivity* $d(\omega)$ [13] as

$$\kappa = \frac{1}{V}\sum_m C(\omega_m)d(\omega_m) = \frac{1}{V}\int_0^\infty d\omega g(\omega)C(\omega)d(\omega), \quad (7)$$

where V is the volume of the system, $g(\omega) = \sum_n \delta(\omega - \omega_n)$ is the density of states, $C(\omega) = k_B(\beta\hbar\omega)^2 e^{\beta\hbar\omega}/(e^{\beta\hbar\omega} - 1)^2$ is the phonon heat capacity, with $\beta \equiv 1/k_B T$ and k_B is the Boltzmann constant. For the classical case, $C(\omega) = k_B$. The heat diffusivity $d(\omega)$, appearing in the above formula, of a normal mode with frequency ω_m and corresponding normalized eigenfunction $\vec{e}_i(m)$ is given by [8,12,13]

$$d(\omega_m, \eta, N) \equiv \frac{\pi}{12\omega_m^2}\sum_{n\neq m}\frac{(\omega_m + \omega_n)^2}{4\omega_m\omega_n}|\vec{\Sigma}_{mn}|^2 f(\omega_n - \omega_m, \eta), \quad (8)$$

where $\vec{\Sigma}_{mn}$ is the heat flux matrix

$$\vec{\Sigma}_{mn} = \sum_{i,j,\alpha,\beta}(\vec{r}_i - \vec{r}_j)e_i^\alpha(m)H_{\alpha\beta}^{ij}e_j^\beta(n), \quad (9)$$

with $H_{\alpha\beta}^{ij}$ is the Hessian matrix elements and $\vec{r}_i$ is the position of the ith particle; $\alpha, \beta = \{x, y, z\}$ are the components. The function $f(\omega_m - \omega_n; \eta) = \eta/\{\pi[(\omega_m - \omega_n)^2 + \eta^2]\}$ is a finite-width representation of the Dirac-δ function that is necessary when dealing with finite systems. The width of the Lorentzian is chosen to be $\eta = \gamma\delta\omega$ with $\gamma > 1$, where $\delta\omega$ is the average spacing between successive modes. Thus, within the harmonic approximation, the density of states $g(\omega)$ and the *thermal diffusivity* $d(\omega)$ are known completely in terms of the eigenvalues and eigenfunctions of the Hessian matrix and using Eq. (7), one can compute the thermal conductivity.

Participation ratio

We expect the diffusivity of modes to depend on their degree of delocalization, which can be quantified by the participation ratio PR(ω). The participation ratio PR(ω) quantifies the localization properties of a normal mode. It is defined as [29],

$$\mathrm{PR}(\omega_n) = \left\{N\sum_{i=1}^{N}[\vec{e}_i(n)\cdot\vec{e}_i(n)]^2\right\}^{-1}. \quad (10)$$

B. Numerical results

We now present the numerical results on the diffusivity, density of states, and participation ratios in our system. As discussed after Eq. (9), for studies of finite systems, we need to regularize the δ functions appearing in the formulas for $d(\omega)$ and $g(\omega)$. With our choice of regularizing function one is required to choose a value for the parameter γ and, as discussed at the end of this section, some of our results are quite sensitive to the choice of the value of γ. For now, we present results for the choice $\gamma = 2.0$.

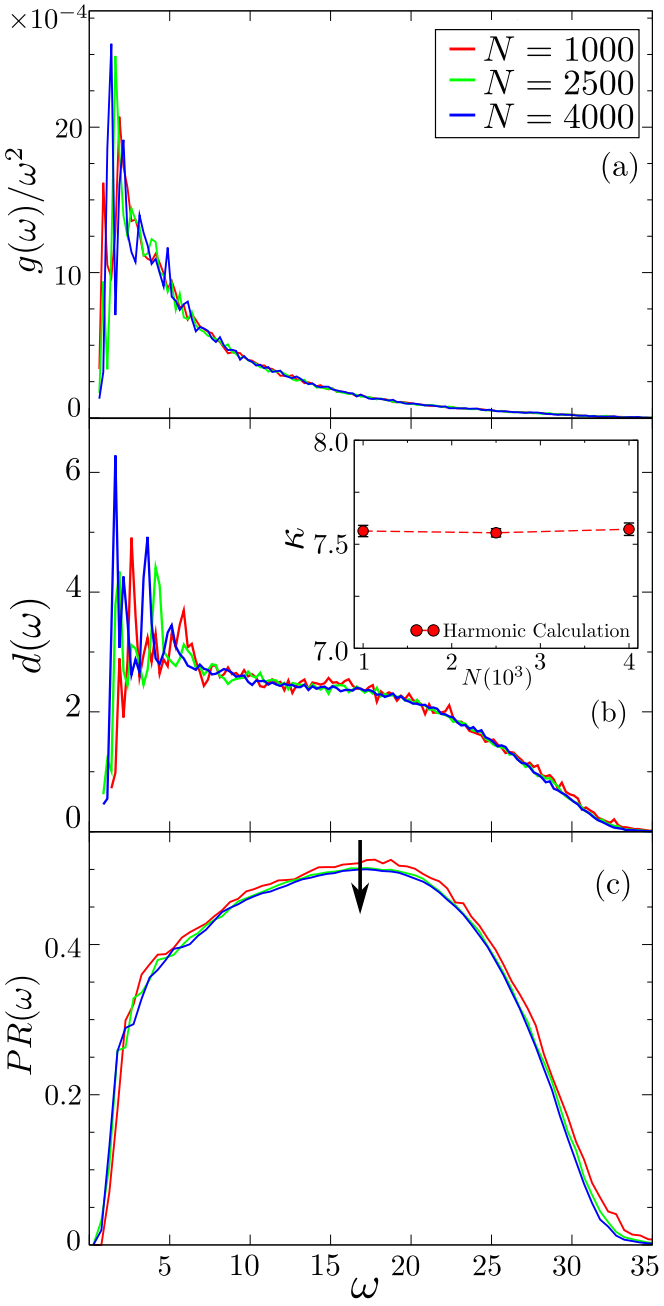

FIG. 7. (a) Reduced density of states $g(\omega)/\omega^2$, (b) heat diffusivity $d(\omega)$, (c) participation ratio PR(ω) for different system sizes with the arrow indicating direction of increasing size. Inset of (b) shows the thermal conductivity κ for three system sizes.

1. Finite-size effects in the harmonic approximation

We take three ISs of average energy levels $\overline{E}_{\rm IS}$ ($= -7.00075 \pm 0.00005$), using a number of different system sizes, and calculate thermal conductivity within the harmonic approximation using Eq. (7). In Fig. 7, we show the corresponding plot for (a) density of states, (b) heat diffusivity, and (c) the participation ratio. In the inset of Fig. 7(b), we show

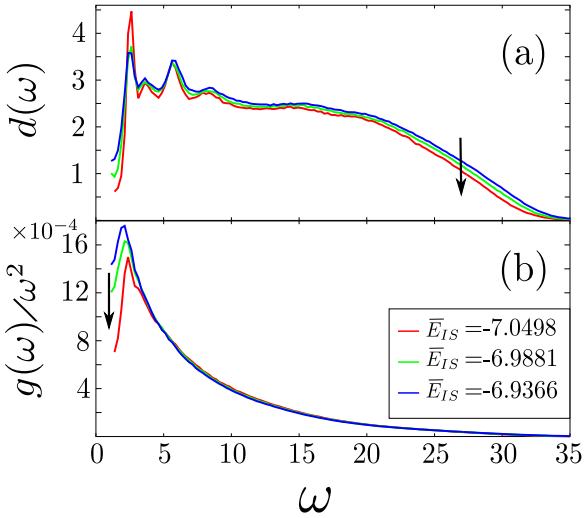

FIG. 8. (a) Heat diffusivity $d(\omega)$ for three different groups of ISs with different $\overline{E}_{\rm IS}$ and (b) density of states $g(\omega)/\omega^2$ showing the increase of extra modes near the boson peak with increase in $\overline{E}_{\rm IS}$. Arrows point to data for lower $\overline{E}_{\rm IS}$ in both plots.

that the finite-size effect on κ is found to be insignificant for these system sizes.

2. Comparison for three different IS energy levels

In Fig. 8, we consider ISs with three different $\overline{E}_{\rm IS}$ having $N = 1\,000$ and compare the results for $d(\omega)$ and $g(\omega)$ for the three cases. As seen in Fig. 8(a), $d(\omega)$ of the ISs with lower $\overline{E}_{\rm IS}$ are smaller over most of the allowed frequency range except for a small region near the boson peak, as compared to the ISs with higher $\overline{E}_{\rm IS}$. We recall that for amorphous solids, excess density of states compared to the Debye law, $g(\omega) \sim \omega^2$, appears in the low-frequency region, and this is known as the boson peak [18]. We find that the boson peak is more pronounced for ISs with higher $\overline{E}_{\rm IS}$ than the ISs with lower $\overline{E}_{\rm IS}$, as shown in Fig. 8(b).

However, the thermal conductivity is a combination of $d(\omega)$, $g(\omega)$, and $C(\omega)$,

$$\kappa(\omega) = \frac{1}{V}\, g(\omega)C(\omega)d(\omega), \tag{11}$$

with $C(\omega) = k_B$, and V is the volume of the system. We have calculated $\kappa(\omega)$ for the three groups of ISs with mean energy $\overline{E}_{\rm IS}$. Fig. 9(a) shows the contribution of the different parts of the vibrational spectrum to the total κ. By performing the sum of $\kappa(\omega)$ over different frequency ranges, we find that the largest contribution to κ comes from the vibrational modes in the middle of the spectrum, where the modes are the most delocalized. However, the maximum contribution to the difference in the value of κ between ISs of different energy is from the modes in the higher end of the vibrational spectrum, as shown in Fig. 9(b), where we plot the numerically computed cumulative integral, $I(\omega) = \int_0^\omega \kappa(\omega')d\omega'$ for the different ISs.

Now, from the participation ratio spectrum PR(ω), shown in Fig. 10, we see that both the low- and high-frequency vibrational modes are more extended for the ISs with higher $\overline{E}_{\rm IS}$. We note here that this trend in the low-frequency regime

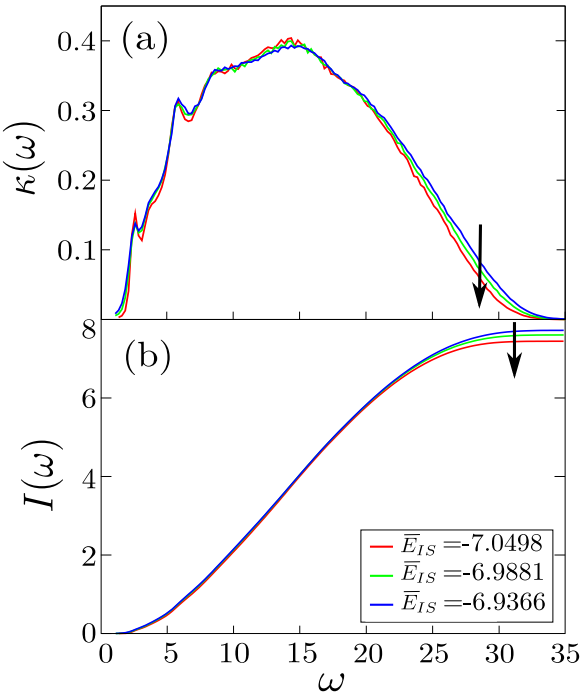

FIG. 9. (a) $\kappa(\omega) = k_B g(\omega)d(\omega)/V$ for three different ISs. (b) Cumulative integral $I(\omega) = \int_0^\omega d\omega'\kappa(\omega')$, showing the contribution of different frequency regime to the overall conductivity, and the variation with $\overline{E}_{\rm IS}$. Arrows point to data for lower $\overline{E}_{\rm IS}$ in both plots.

is consistent with recent studies [32,33], where it has been observed that localization properties of quasilocalized modes have a similar dependence on preparation history.

Since the main contribution in the difference in κ for different $\overline{E}_{\rm IS}$ comes mainly from the higher end of the frequency spectrum, as discussed above, we can conclude that increased thermal conductivity with increasing $\overline{E}_{\rm IS}$ is related to the increased delocalization of these vibrational modes, with the high-frequency modes playing a more important role.

3. Dependence of $d(\omega)$ on the value of γ

The value of heat diffusivity, $d(\omega)$, calculated via harmonic analysis, is sensitive to the choice of γ, the width of the

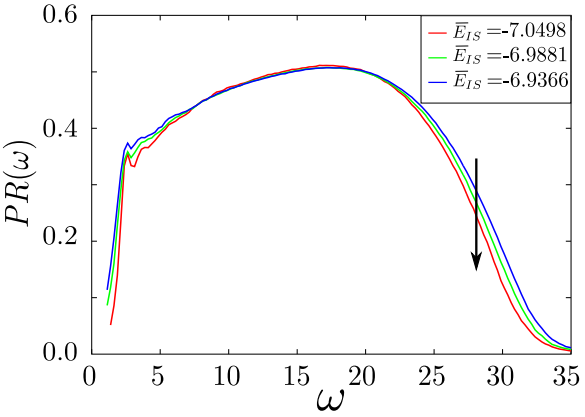

FIG. 10. Participation ratio showing the presence of more localized low and high-frequency modes with decreasing $\overline{E}_{\rm IS}$ (arrow pointing to data for lower $\overline{E}_{\rm IS}$).

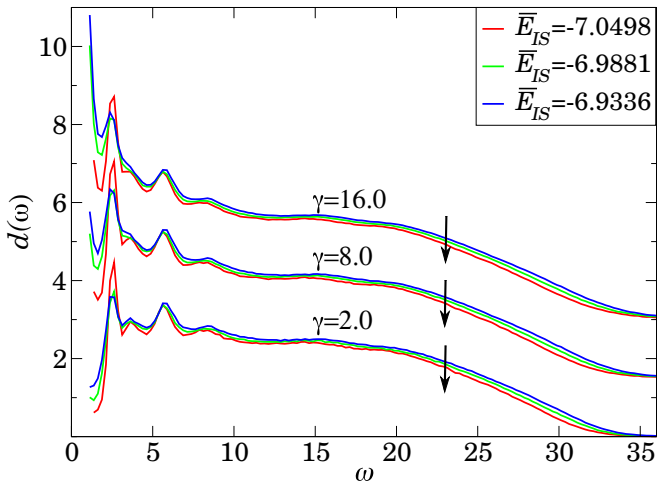

FIG. 11. Heat diffusivity $d(\omega)$ for three different groups of ISs with different $\overline{E}_{\rm IS}$ (arrows pointing to data for lower $\overline{E}_{\rm IS}$) for three different values of γ. For convenience of comparsion the values of $d(\omega)$ for $\gamma = 8.0$ and 16.0 has been shifted by 1.5 and 3.0, respectively.

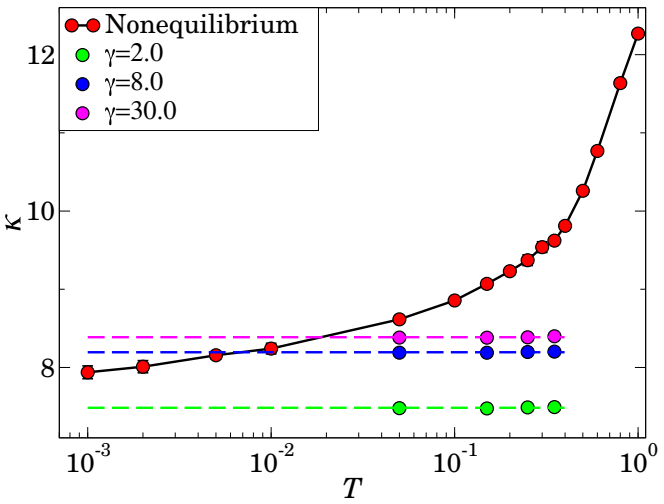

FIG. 12. Thermal conductivity (κ) for different temperatures from nonequilibrium simulation at cooling rate 3.33×10^{-6}. The horizontal dashed lines along with the points show the values of κ calculated in harmonic approximation, sampling ISs at few low temperatures, for three different values of γ.

broadening function. In Fig. 11, we show the dependence of $d(\omega)$ on γ for the three different groups of ISs considered in Sec. IV B 2. The nature of the dependence of $d(\omega)$ on the IS energy does not change with changing γ for most values of ω, except at the low-frequency end where numerical artifacts start appearing because of the overestimation in the density of states for higher values of γ. All results in this section have been reported for $\gamma = 2$.

4. Comparison of κ values from nonequilibrium simulation and harmonic calculation

As illustrated in Sec. IV B 3, the values of $d(\omega)$ and consequently the thermal conductivity, κ, calculated from the harmonic calculation is sensitive to the choice of γ. To obtain the true κ, one needs to take the $N \to \infty$, $\eta \to 0$ limit. For finite systems, the choice of γ leads to some uncertainty in the calculated κ, and it is not clear what the optimal choice of η should be, to extract the true thermal conductivity. In Fig. 12, we compare the values of κ at low temperatures obtained from nonequilibrium simulation to those obtained from harmonic calculation performed with three different choices of γ from ISs derived at few low temperatures. The "correct" value of γ can not be determined precisely from the results shown in this figure.

C. Direct numerical verification of the harmonic approximation at low temperatures

One can ask whether at low temperatures the system actually stays within the basin of a given IS (a local minimum of the potential) and also if nonlinear effects are important for dynamics within the basin of an IS. Here we examine this question of the validity of the harmonic approximation at low temperatures. Our first finding is that even at as low temperatures as $T = 0.002$, the system can move between potential energy basins that are characteized by different IS energies. To see this we start with the system in a given IS (specified by $E_{\rm IS}$) and then, after evolving it for a fixed long time interval, we re-computed the $E_{\rm IS}$. We found that depending on how low the initial $E_{\rm IS}$ was, a significant fraction of trajectories moved out to different wells. For the lowest energies, this was for around 15% of all cases, while for higher energies, as much as 60% trajectories moved to different wells. In the former case, the new IS configuration differed from the starting configuration by displacements of a small number of particles while in the latter case this involved large rearrangements.

We now focus on the cases where the system does remain confined in a given well for the duration of observation. For these cases, we computed and compared the energy current auto-correlation function $C(t) = \langle \vec{\mathcal{J}}(0) \cdot \vec{\mathcal{J}}(t) \rangle$, at $T = 0.002$, using molecular dynamics with the actual interactions and within the harmonic approximation for an IS.

In the harmonic theory, the total energy of an equilibrium state at temperature T is $\overline{E}_{\rm IS} + [(6N-3)k_BT/2]$. We prepare an initial state by choosing positions corresponding to an IS and giving each particle a random velocity taken from a Maxwell distribution at a temperature $2T$. Within a short span of time, the equipartioning of energy occurs. With these initial conditions, we first perform MD simulations with the full interparticle potential (normal simulation) and, second, with the interparticle forces replaced by the forces from the Hessian elements (Hessian simulation). We consider only those low energy ISs for which the system stays inside the initial basin during the course of the simulation. The results are shown in Fig. 13. We see excellent agreement between the two which implies that the harmonic approximation is indeed quite accurate at this temperature, for the cases where the system remains within a given potential well. This then supports the explanation of Fig. 6 based on the harmonic approximation given in the previous section.

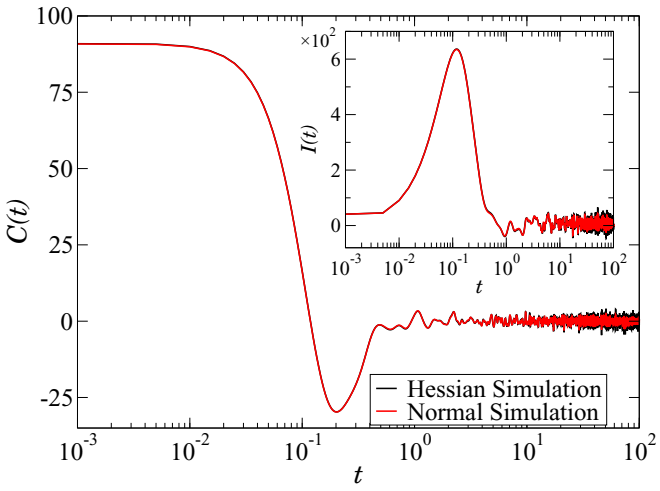

FIG. 13. Current autocorrelation function $C(t)$ and its integral $I(t)$, shown in the inset, calculated from normal and Hessian simulations for a system with $N = 1\,000$, at $T = 0.002$.

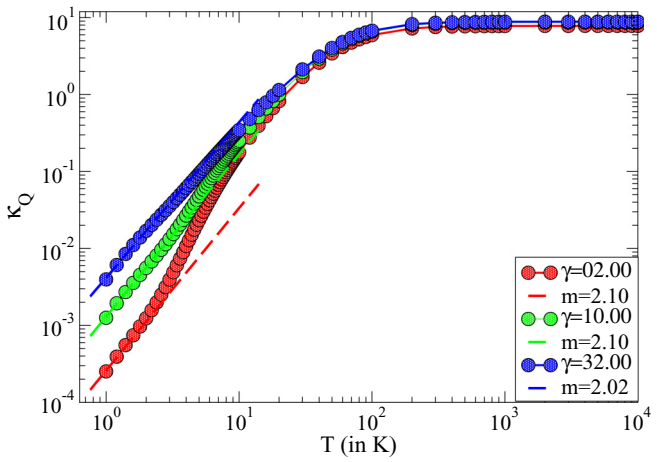

FIG. 14. Quantum thermal conductivity κ_Q as a function of temperature. As discussed in Sec. III due to the uncertainty associated with γ, κ_Q depends on the value of γ, nevertheless, it follows a nearly T^2 rise. The closed circles denote the values of κ_Q computed at different temperatures for three different values of γ, and the associated dashed lines show power-law fits to the low-T data with m signifying the exponent of the power law.

D. Quantum effects

The effects of quantum correction to the thermal conductivity of a system can be approximated by using the vibrational density of states [10]. For our simulation system, the physical units of length, energy and time used are $\sigma = 2.218$ Å, $\epsilon/k_B = 933.26$ K and $\tau = 0.627$ ps, respectively [22,34]. The debye temperature T_D is calculated from the relation $T_D = \hbar\omega_D/k_B$, where ω_D is the Debye frequency of the system. ω_D is estimated from the relation,

$$3N = \frac{V}{2\pi^2}\frac{\omega_D^3}{3}\left[\frac{2}{v_T^3} + \frac{1}{v_L^3}\right], \tag{12}$$

where N is the number of particles, V is the volume of the system, and v_T and v_L are the longitudinal and transverse sound speed respectively, with values of 45.58×10^2 m/s and 19.08×10^2 m/s. (Details of our estimation of the sound speeds are given in Appendix 2.)

Temperature dependence

For our system, we have estimated that $\omega_D \sim 26.89 \times 10^{12}$ Hz and $T_D \sim 196$ K. We have computed the approximate quantum thermal conductvity of the system for a bunch of ISs using Eq. (7). Figure 14 shows the values of quantum thermal conductivity for three different values of γ. It is clear from the figure that, quantum effects are quite important upto the value of the Debye temperature, that is estimated above. At high temperatures, the quantum thermal conductivity saturates to its classical limit. At low temperatures k_Q shows a nearly T^2 rise.

V. CONCLUSIONS AND DISCUSSION

Using numerical simulations, we have studied thermal transport in a model glass-forming liquid. The values of the thermal conductivity, obtained from nonequilibrium and Green-Kubo calculations are found to agree well over a wide range of temperatures. One of our main findings is that the phenomenon of *aging* has a significant effect on thermal transport. Near the glass transition temperature, the conductivity drops considerably with increasing age. Similarly, the conductivity of the low temperature glasses can vary by about 10% depending on the cooling protocol used to form it.

The lowering of conductivity with growing age or slower cooling can be rationalised in terms of the system exploring lower energy minima. Our numerical results demonstrate that the thermal conductivity increases linearly with the energy of the IS. We also performed an analysis of the harmonic solid associated with the ISs, through an examination of the diffusivity and participation ratio of the normal modes. This analysis suggests that an explanation, of the dependence of conductivity on energy of ISs, could be that the extent of localization of the normal modes is higher for the lower energy IS. We mostly studied the classical case, but some interesting features in the quantum regime, obtained from the harmonic approximation, are briefly discussed.

We close with a discussion of possible problems arising from the use of relatively small samples and fast cooling rates in our work. This is an inherent problem of all numerical work—one can always argue that the use of larger samples and longer simulation times may give different results. The important issue here is whether some of the reported numerical results are robust in the sense that they are expected to remain valid in the limit of long time and large system size. We believe that some of the important results reported in our paper are robust in this sense.

The thermal properties of glasses at low temperatures are affected by several different kinds of excitations. In particular, quasilocalized soft modes [32] are expected to play an important role. The system sizes considered in our study are perfectly adequate [35] for studying the contribution of these modes to the thermal conductivity. Our results for this contribution are internally consistent: the results for the thermal conductivity obtained from two different calculations (nonequilibrium and Green-Kubo) agree with each other [see

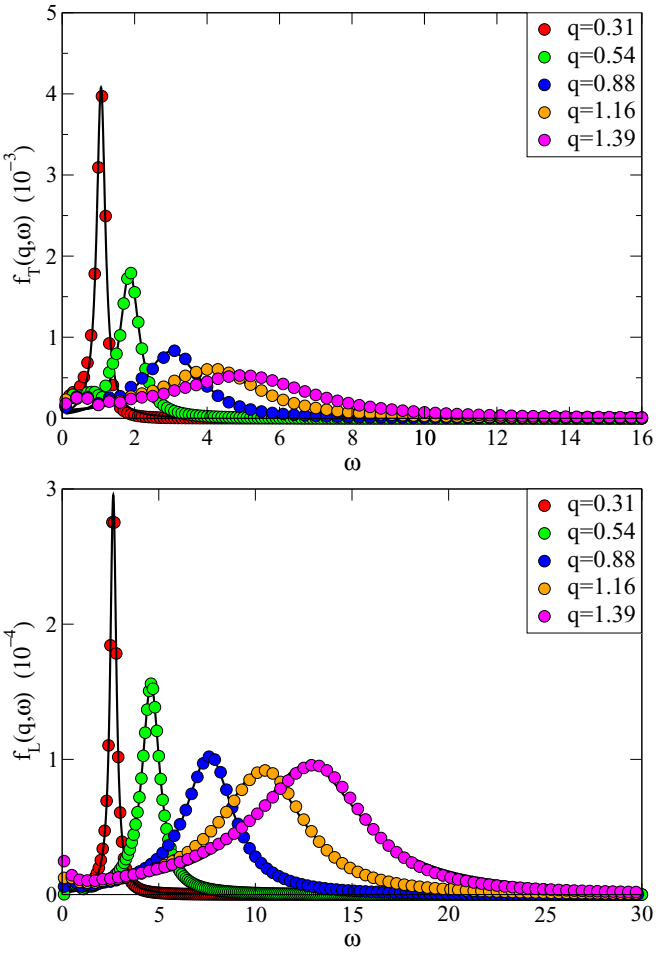

FIG. 15. (Top) $f_T(q,\omega)$ as a function of ω at few values of q. (Bottom) $f_L(q,\omega)$ as a function of ω. q increases from left to right in both plots. The filled circles are the data and the filled lines are the corresponding Lorentzian fit. The data is for $N = 10\,000$.

Fig. 5(a)] and we have checked for convergence with system size [see inset in Fig. 5(a)]. These results can be understood from the properties of harmonic excitations of appropriate ISs. Several qualitative features of our results are robust and not artifacts of considering very small systems. We note that indeed we cannot rule out the possibility that long-wavelength phonons might still affect our results for much larger systems—however, our results would be applicable to physical systems with random pinning [36] in which long-wavelength phonon modes are suppressed. The relatively fast cooling rates used in our simulations should not be a concern because the crucial feature responsible for our main conclusion (higher degree of localization of the eigenmodes for ISs with lower energy) is also found in studies of very low-energy ISs [33].

Regarding the role of long-wavelength phononlike excitations, phononlike modes are indeed present in the samples considered in our study (see Fig. 15). Our calculation of the thermal conductivity in the harmonic approximation does take into account the contributions of these modes. However, our calculations also show that the contribution of these modes does not dominate over those of other modes—the dependence of the thermal conductivity on the IS energy actually arises from the localization properties of higher frequency modes [see Fig. 9(b)]. An important question is whether this would continue to be true if much larger systems, in which phonons with longer wavelengths would be present, are considered.

The question of whether the dependence of the lifetime τ of phonons on the wavenumber k follows the Rayleigh scattering form [37], $\tau(k) \propto 1/k^4$ in three dimensions, is important in this context. The contribution of long-wavelength phonons to the thermal conductivity in the harmonic approximation would diverge if the Rayleigh scattering form is valid. This follows since the low-frequency diffusivity is given by $d(\omega) \approx c(\omega)\ell(\omega)$, where $c(\omega)$ is the speed of sound and $\ell(\omega)$ is the mean free path that would diverge as $1/\omega^4$ as $\omega \to 0$. Since the phonon density of states $g(\omega)$ in three dimensions is proportional to ω^2, this will cause the integral $\int d\omega g(\omega) d(\omega)$ to blow up. Indeed this has been seen in some earlier studies [13,30,38] but for systems with zero stress, whereas the inherent structures used in our harmonic calculation have finite stresses. Recent numerical studies [39–41] have provided fairly convincing evidence in support of the validity of the Rayleigh scattering form. This seems to indicate that the contribution of the long-wavelength phonon modes indeed dominates the thermal conductivity. This argument, however, is not conclusive because it is based on the *validity of the harmonic approximation*. In real glasses at finite temperatures, anharmonic effects, arising from interactions among the harmonic modes and transitions between ISs that differ from each other by changes in the positions of a few particles, are expected to change the k-dependence of the phonon lifetime from the Rayleigh form. As mentioned above, we see transitions to the basins of other ISs even when the temperature is very low. In a recent paper [42], it has been argued that localized excitations that allow the system to access different ISs are present even deep in the equilibrium glass state. Such excitations, known as "two-level systems" [3] are believed to play an important role in the temperature dependence of the specific heat of glasses at low temperatures. The experimentally measured thermal conductivity of glasses is, of course, finite (it appears to vanish as the temperature approaches zero). Therefore, the prediction of the harmonic theory about the divergent contribution of long-wavelength phonons to the thermal conductivity should not be taken seriously and there is no strong argument in support of the view that the thermal conductivity at low temperatures is dominated by the contribution of long-wavelength phonons.

In Ref. [39], it was shown that the mean free path in the harmonic regime at phononic frequencies (extracted from phonon life times) increases as the level of annealing is increased. The same behavior is seen also in our simulations [see Fig. 17]. In spite of that, we find that the conductivity κ is lower for ISs with lower energy. This suggests that low-frequency phonon contribution to the thermal conductivity does not dominate over the contributions from all other modes. If this continues to remain valid for large well-annealed systems, then the observation of Ref. [39] would not invalidate our conclusion about the dependence of the thermal conductivity on the degree of annealing. It should also be noted that there is no proof of the connection between the thermal diffusivity that

we compute from the Hessian matrix of the disordered system, and the mean free path that one extracts from the phonon life time. Relating the thermal conductivity of the sample to the phonon life time is a naive kinetic theory expectation, which needs to be established for the strongly disordered structures that we are looking at.

To summarize, our results show that the low-temperature thermal conductivity of systems in which long wavelength phonon modes are suppressed (e.g., in glasses with random pinning [36]) decreases as the degree of annealing is increased. A definitive answer to the subtle question of whether the presence of long wavelength phonon modes would change this behavior requires an understanding of anharmonic affects which are difficult to study analytically or numerically. More work in this direction, especially experimental investigations of the thermal conductivity of glasses with different levels of annealing [43], would be most welcome.

ACKNOWLEDGMENTS

We thank J.-L. Barrat and J. Horbach for discussions; D. Banerjee and H. Khare for their help with figures. P.J.B. and R.M. acknowledge financial support from CSIR, India. We thank SERC IISc, IMSc, and ICTS for computing support. A.D. acknowledges support from the Indo-Israel joint research Project No. 6-8/2014(IC) and from the French Ministry of Education through the grant ANR (EDNHS). C.D. acknowledges support from Department of Science & Technology (DST), India.

APPENDIX

1. Low-frequency phononlike modes

Within the harmonic approximation, the structure of the normal modes in a system can be studied via the dynamical structure factor (transverse and longitudinal) calculated in the limit of one excitation approximation using the following expression [44,45],

$$S_\alpha(q,\omega) = \frac{k_B T}{M}\frac{q^2}{\omega^2}\sum_\lambda E_{\lambda,\alpha}(q)\delta(\omega-\omega_\lambda), \tag{A1}$$

where α represents transverse or longitudinal modes.

For transverse modes,

$$E_{\lambda,T}(q) = \frac{1}{N}\left|\sum_i [\hat{\mathbf{q}}\times\vec{\mathbf{e}}_\lambda(i)]\exp(i\vec{\mathbf{q}}.\vec{\mathbf{r}}_i)\right|^2, \tag{A2}$$

and for longitudinal modes,

$$E_{\lambda,L}(q) = \frac{1}{N}\left|\sum_i [\hat{\mathbf{q}}\cdot\vec{\mathbf{e}}_\lambda(i)]\exp(i\vec{\mathbf{q}}.\vec{\mathbf{r}}_i)\right|^2. \tag{A3}$$

For simplicity we compute the functions $f_T(q,\omega) = \langle E_{\lambda,T}(q)\delta(\omega-\omega_\lambda)\rangle$ and $f_L(q,\omega) = \langle E_{\lambda,T}(q)\delta(\omega-\omega_\lambda)\rangle$ [13], coarse-grained in frequency domain, using frequency-binning of 0.1. The dispersion and the associated width can be measured by taking an approximate Lorentzian line shape for $f_T(q,\omega)$ and $f_L(q,\omega)$ [46]. Alternatively, the dynamical structure factor data can be fitted to a damped harmonic oscillator model to extract the same quantities. We have verified that within the limit of numerical accuracy these two approaches give similar results for small q values, which was also shown by Schober [47].

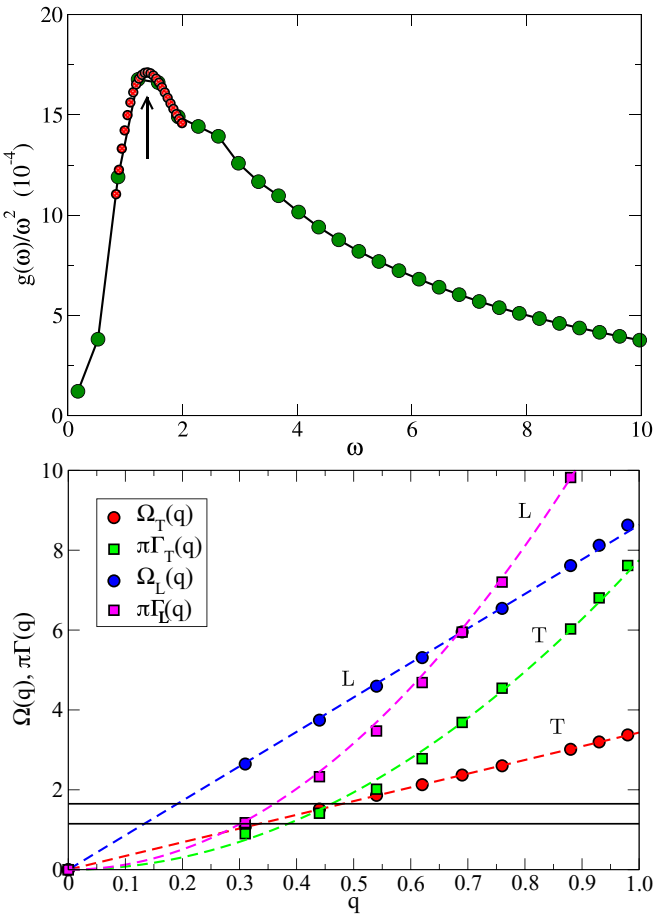

FIG. 16. $N = 1\,000$. (Top) Reduced density of states $g(\omega)/\omega^2$ showing presence of boson peak. The peak region has been fitted to a polynomial to locate the peak frequency, the upward arrow shows the position of the boson peak frequency ω_{BP}. (Bottom) dispersion relation Ω_α and $\pi\Gamma_\alpha$ (where, α is L or T for longitudinal or transverse modes respectively). The filled circles show Ω_α while the associated dashed lines are fits to q. The filled squares show $\pi\Gamma_\alpha$ with the associated dashed curves showing fits to q^2. The two horizontal black lines shows the region where the boson peak frequency lies. It is observed that, the Ioffe-Regel frequency (where the Ω_α line and $\pi\Gamma_\alpha$ curve intersect) for the transverse waves coincide with the boson peak frequency, while Ioffe-Regel frequency for the longitudinal waves is higher than the boson peak frequency.

2. Ioffe-Regel frequency

In Fig. 15 we show $f_T(q,\omega)$ and $f_L(q,\omega)$ as a function of ω for few small q values. These can be fitted to a Lorentzian using the following form [46,48]:

$$S(q,\omega) \propto \frac{\Gamma(q)/2}{[\omega-\Omega(q)]^2 + [\Gamma(q)/2]^2}, \tag{A4}$$

where $\Omega(q)$ is the position of the peak and $\Gamma(q)$ is the width. From the fits of $f_T(q,\omega)$ and $f_L(q,\omega)$, we determine the phonon-dispersion relation for the transverse and longitudinal modes. The dispersion [$\Omega(q)$ versus q] can be fitted well to

straight lines for much of the small q-values, slopes of which provide the transverse and longitudinal sound speeds (v_T and v_L) from their respective dispersion. The width $\Gamma(q)$ can be fitted by q^2. This is in agreement with analytic [49], numerical [39], and experimental [43] results for modes with frequency near that of the Boson peak.

The Ioffe-Regel limit for phonons is reached when their mean free path decreases to their wavelength [50]; i.e., $2\pi\Gamma(q)/2 \approx \Omega(q)$ [46,48]. In Fig. 16 (bottom) we show the dispersion relation and the width for transverse and longitudinal modes. We have estimated the boson peak frequency from the reduced density of states $g(\omega)/\omega^2$ as shown in Fig. 16 (top). From the intersection of the dispersion and the $\pi\Gamma_\alpha$ data, the Ioffe-Regel frequency can be located. We find that the Ioffe-Regel frequency for the transverse modes coincides with the boson peak frequency. Similar results were reported in earlier works involving Lennard-Jones [45] and soft-sphere systems [46], and this finding is different from the observation of Xu *et al.* for the jammed Hertzian spheres [13] where the Ioffe-Regel frequency is smaller than the Boson peak frequency. In general, it is hypothesized that the relationship between these two frequencies could depend upon the microscopic structure of the glass [49].

3. Dependence of $\Omega(q)$ and $\Gamma(q)$ on $\overline{E}_{\rm IS}$

In Fig. 17 the dispersion relation and the associated width for the three groups of ISs are shown. We find that, within the limit of numerical accuracy involving fitting, the dispersion relations for the three groups of ISs give similar values of speed of sound (transverse and longitudinal). The damping factor shows a weak dependence on $\overline{E}_{\rm IS}$—it decreases as the IS energy is decreased, indicating that the phonon lifetime is larger for ISs with lower energy. This is in agreement with the results reported in Ref. [39]. If interpreted naively, this result would imply that the thermal conductivity should increase with the degree of annealing. However, we find that the conductivity is lower for inherent structures with lower energy. This observation suggests that the contribution of low-frequency phonons to the thermal conductivity does not dominate over the contributions of other modes.

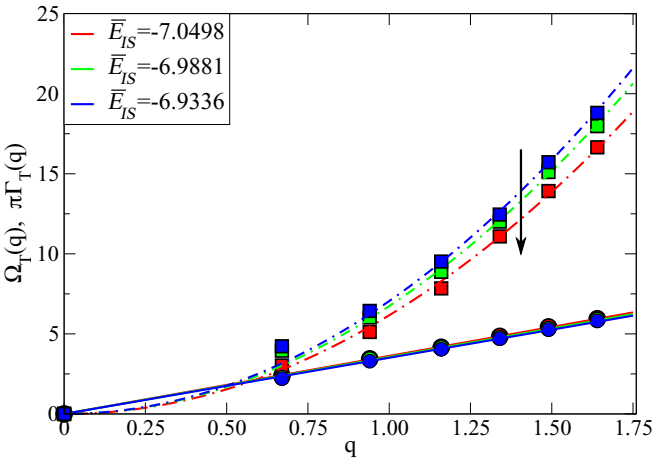

FIG. 17. Dispersion relation and $\pi\Gamma_T$ for the transverse waves, for the three groups of ISs (arrow pointing to data for lower $\overline{E}_{\rm IS}$). The filled circles are Ω_T fitted by q (thick solid line) and the filled squares are $\pi\Gamma_T$ fitted by q^2 (dashed-dotted curve). The data is for the system with $N = 1\,000$ presented in the main text.

[1] D. G. Cahill and R. O. Pohl, Annu. Rev. Phys. Chem. **39**, 93 (1988).
[2] R. C. Zeller and R. O. Pohl, Phys. Rev. B **4**, 2029 (1971).
[3] P. W. Anderson, B. I. Halperin, and C. M. Varma, Philos. Mag. **25**, 1 (1972).
[4] C. C. Yu and J. J. Freeman, Phys. Rev. B **36**, 7620 (1987).
[5] U. Buchenau, Y. M. Galperin, V. L. Gurevich, D. A. Parshin, M. A. Ramos, and H. R. Schober, Phys. Rev. B **46**, 2798 (1992).
[6] V. Lubchenko and P. G. Wolynes, Proc. Natl. Acad. Sci. USA **100**, 1515 (2003).
[7] W. Schirmacher, Europhys. Lett. **73**, 892 (2006).
[8] V. Vitelli, N. Xu, M. Wyart, A. J. Liu, and S. R. Nagel, Phys. Rev. E **81**, 021301 (2010).
[9] A. Marruzzo, W. Schirmacher, A. Fratalocchi, and G. Ruocco, Sci. Rep. **3**, 1407 (2013).
[10] H. Mizuno, S. Mossa, and J. L. Barrat, Phys. Rev. B **94**, 144303 (2016).
[11] P. B. Allen and J. L. Feldman, Phys. Rev. Lett. **62**, 645 (1989).
[12] P. B. Allen and J. L. Feldman, Phys. Rev. B **48**, 12581 (1993).
[13] N. Xu, V. Vitelli, M. Wyart, A. J. Liu, and S. R. Nagel, Phys. Rev. Lett. **102**, 038001 (2009).
[14] M. Wyart, Europhys. Lett. **89**, 64001 (2010).
[15] H. Mizuno, S. Mossa, and J. L. Barrat, Europhys. Lett. **104**, 56001 (2013)
[16] W. Kob and J. L. Barrat, Phys. Rev. Lett. **78**, 4581 (1997).
[17] K. Vollmayr, W. Kob, and K. Binder, J. Chem. Phys. **105**, 4714 (1996).
[18] K. Binder and W. Kob, *Glassy Materials and Disordered Solids: An Introduction to Their Statistical Mechanics* (World Scientific, Singapore, 2011).
[19] Y. Shi and M. L. Falk, Phys. Rev. B **73**, 214201 (2006).
[20] R. L. Moorcroft, M. E. Cates, and S. M. Fielding, Phys. Rev. Lett. **106**, 055502 (2011).
[21] G. P. Shrivastav, P. Chaudhuri, and J. Horbach, J. Rheol. **60**, 835 (2016).
[22] W. Kob and H. C. Andersen, Phys. Rev. Lett. **73**, 1376 (1994).
[23] S. Sastry, P. G. Debenedetti, and F. H. Stillinger, Nature **393**, 554 (1998)
[24] J. P. Hansen and I. R. McDonald, *Theory of Simple Liquids*, 3rd ed. (Academic Press, London, 2006).
[25] P. Scheidler, W. Kob, A. Latz, J. Horbach, and K. Binder, Phys. Rev. B **63**, 104204 (2001).
[26] F. Sciortino, W. Kob, and P. Tartaglia, Phys. Rev. Lett. **83**, 3214 (1999).
[27] T. B. Schröder, S. Sastry, J. C. Dyre, and S. C. Glotzer, J. Chem. Phys. **112**, 9834 (2000).
[28] C. Rainone, A. Moriel, G. Kapteijns, E. Bouchbinder, and E. Lerner, arXiv:1902.06225.

[29] B. B. Laird and H. R. Schober, Phys. Rev. Lett. **66**, 636 (1991).
[30] A. Kundu, A. Chaudhuri, D. Roy, A. Dhar, J. L. Lebowitz, and H. Spohn, Europhys. Lett. **90**, 40001 (2010).
[31] S. R. Nagel, G. S. Grest, and A. Rahman, Phys. Rev. Lett. **53**, 368 (1984).
[32] E. Lerner, G. Düring, and E. Bouchbinder, Phys. Rev. Lett. **117**, 035501 (2016).
[33] L. Wang, A. Ninarello, P. Guan, L. Berthier, G. Szamel, and E. Flenner, Nat. Commun. **10**, 26 (2019).
[34] T. A. Weber and F. H. Stillinger, Phys. Rev. B **31**, 1954 (1985).
[35] G. Kapteijns, E. Bouchbinder, and E. Lerner, Phys. Rev. Lett. **121**, 055501 (2018).
[36] L. Angelani, M. Paoluzzi, G. Parisi, and G. Ruocco, Proc. Nat. Acad. Sci. USA **115**, 8700 (2018).
[37] J. M. Ziman, *Principles of the Theory of Solids* (Cambridge University Press, Cambridge, 1972).
[38] A. Chaudhuri, A. Kundu, D. Roy, A. Dhar, J. L. Lebowitz, and H. Spohn, Phys. Rev. B **81**, 064301 (2010).
[39] L. Wang, L. Berthier, E. Flenner, P. Guan, and G. Szamel, Soft Matter **15**, 7018 (2019).
[40] A. Moriel, G. Kapteijns, C. Rainone, J. Zylberg, E. Lerner, and E. Bouchbinder, J. Chem. Phys. **151**, 104503 (2019).
[41] H. Mizuno and S. Mossa, Condens. Matter Phys. **22**, 43604 (2019).
[42] M. Ozawa, A. Ikeda, K. Miyazaki, and W. Kob, Phys. Rev. Lett. **121**, 205501 (2018).
[43] E. A. A. Pogna, A. I. Chumakov, C. Ferrante, M. A. Ramos, and T. Scopigno, J. Phys. Chem. Lett. **10**, 427 (2019).
[44] M. Sampoli, P. Benassi, R. Dell'Anna, V. Mazzacurati, and G. Ruocco, Philos. Mag. **77**, 473 (1998).
[45] H. Shintani and H. Tanaka, Nat. Mater. **7**, 870 (2008).
[46] H. R. Schober and C. Oligschleger, Phys. Rev. B **53**, 11469 (1996).
[47] H. R. Schober, J. Phys. Condens. Matter **16**, S2659 (2004).
[48] S. N. Taraskin and S. R. Elliott, Phys. Rev. B **61**, 12017 (2000).
[49] E. DeGiuli, A. Laversanne-Finot, G. Düring, E. Lerner, and M. Wyart, Soft Matter **10**, 5628 (2014).
[50] V. L. Gurevich, D. A. Parshin, J. Pelous, and H. R. Schober, Phys. Rev. B **48**, 16318 (1993).